doi:10.1093/brain/awr093 Brain 2011: 134; 1610–1622 | 1610

BRAIN
A JOURNAL OF NEUROLOGY

Disability, atrophy and cortical reorganization following spinal cord injury

Patrick Freund,[1,2,3,4] Nikolaus Weiskopf,[2] Nick S. Ward,[5] Chloe Hutton,[2] Angela Gall,[3] Olga Ciccarelli,[1] Michael Craggs,[3] Karl Friston[2] and Alan J. Thompson[1]

1 Department of Brain Repair and Rehabilitation, UCL Institute of Neurology, UCL, WC1N 3BG London, UK
2 Wellcome Trust Centre for Neuroimaging, UCL Institute of Neurology, UCL, WC1N 3BG London, UK
3 Spinal Cord Injury Centre, Royal National Orthopaedic Hospital, UCL, HA7 4LP London, UK
4 Swiss Paraplegic Research, CH-6207 Nottwil, Switzerland
5 Sobell Department of Motor Neuroscience, UCL Institute of Neurology, UCL, WC1N 3BG London, UK

Correspondence to: Patrick Freund,
Department of Brain Repair and Rehabilitation,
UCL Institute of Neurology,
UCL, Queen Square,
London WC1N 3BG, UK
E-mail: p.freund@ion.ucl.ac.uk

The impact of traumatic spinal cord injury on structural integrity, cortical reorganization and ensuing disability is variable and may depend on a dynamic interaction between the severity of local damage and the capacity of the brain for plastic reorganization. We investigated trauma-induced anatomical changes in the spinal cord and brain, and explored their relationship to functional changes in sensorimotor cortex. Structural changes were assessed using cross-sectional cord area, voxel-based morphometry and voxel-based cortical thickness of T_1-weighted images in 10 subjects with cervical spinal cord injury and 16 controls. Cortical activation in response to right-sided (i) handgrip; and (ii) median and tibial nerve stimulation were assessed using functional magnetic resonance imaging. Regression analyses explored associations between cord area, grey and white matter volume, cortical activations and thickness, and disability. Subjects with spinal cord injury had impaired upper and lower limb function bilaterally, a 30% reduced cord area, smaller white matter volume in the pyramids and left cerebellar peduncle, and smaller grey matter volume and cortical thinning in the leg area of the primary motor and sensory cortex compared with controls. Functional magnetic resonance imaging revealed increased activation in the left primary motor cortex leg area during handgrip and the left primary sensory cortex face area during median nerve stimulation in subjects with spinal cord injury compared with controls, but no increased activation following tibial nerve stimulation. A smaller cervical cord area was associated with impaired upper limb function and increased activations with handgrip and median nerve stimulation, but reduced activations with tibial nerve stimulation. Increased sensory deficits were associated with increased activations in the left primary sensory cortex face area due to median nerve stimulation. In conclusion, spinal cord injury leads to cord atrophy, cortical atrophy of primary motor and sensory cortex, and cortical reorganization of the sensorimotor system. The degree of cortical reorganization is predicted by spinal atrophy and is associated with significant disability.

Keywords: spinal cord injury; atrophy; cortical reorganization; disability

Abbreviations: ARAT = Arm Research Action Test; BOLD = blood oxygenation level-dependent; SCI = spinal cord injury; VBCT = voxel-based cortical thickness; VBM = voxel-based morphometry

Received August 11, 2010. Revised February 13, 2011. Accepted March 28, 2011

Introduction

Traumatic spinal cord injury (SCI) usually leads to permanent clinical impairment and is a life changing event (Dietz and Curt, 2006). Currently there is no 'cure' for paralysis. However, recent discoveries, such as anti-Nogo-A antibody treatment (Schwab, 2002), have the potential to translate into therapies with patient benefit (Freund *et al*., 2006), but their efficacy depends on carefully designed clinical trials. Consequently, there is a prescient need to develop non-invasive biomarkers, which quantify the impact of SCI upon the structural integrity and functional reorganization of sensorimotor systems and the ensuing clinical impairment. For example, in other diseases such as multiple sclerosis, changes in whole-brain volume, which reflect the development of atrophy, have been used to quantify treatment effects (Barkhof *et al*., 2010).

The development of accurate and sensitive biomarkers depends largely on fundamental understanding of the pathophysiological events following spinal injury. Extensive studies of animal models have elucidated major pathophysiological mechanisms due to SCI and regenerative mechanisms of recovery (Schwab, 2002). SCI causes disintegration of axons and disrupts pathways mediating efferent and afferent information flow between the brain and spinal cord. However, the majority of affected neurons survive (Hains *et al*., 2003; Beaud *et al*., 2008) and remain receptive to synaptic input (Tseng and Prince, 1996). Regenerative sprouting of axons is a potential mechanism for functional reintegration of injured neurons into sensory–motor circuits (Bareyre *et al*., 2004). Furthermore, this sprouting may enhance access to neurotrophic support, supporting cell survival and contributing to cortical reorganization.

It is not fully understood how these mechanisms relate to SCI in humans, since studies in humans require non-invasive approaches that have only been available recently. Following SCI, human patients show spinal atrophy (Freund *et al*., 2009; Lundell *et al*., 2010*a*), cortical atrophy (Jurkiewicz *et al*., 2006; Wrigley *et al*., 2009*a*) and cortical reorganization in the sensorimotor cortex (for review see Kokotilo *et al*., 2009). Specifically, subjects with SCI who recover functionally (Jurkiewicz *et al*., 2007) or who undergo surgical decompression (Duggal *et al*., 2010) show increases in the volume of activation in primary motor cortex. Increased cerebral activation during lower limb movement is correlated with spinal atrophy and impairment assessed by the American Spinal Injury Associations score (Lundell *et al*., 2010*b*). Analogously, subjects with SCI who do not recover show a reduced volume of activation in primary motor cortex (Jurkiewicz *et al*., 2010).

The effects of spinal cord trauma on white matter volume and cortical thickness have not been investigated. Furthermore, the relationship between SCI-related anatomical changes, hand function and cortical reorganization of the sensorimotor cortex is not well understood. Understanding of this complex interaction is important for a principled development of biomarkers, prognosis and clinical trials for spinal cord repair (Ellaway *et al*., 2010). To explore this relationship, we assessed non-invasively the extent of anatomical changes and its effect on cortical reorganization in chronic subjects with SCI. We measured cross-sectional cord area proximal to the site of injury (Freund *et al*., 2010). We then investigated the extent of degenerative changes in white and grey matter volume in cortical and subcortical regions of interest of the corticospinal system, as measured by voxel-based morphometry (VBM) (Ashburner *et al*., 2003) and voxel-based cortical thickness (VBCT) (Hutton *et al*., 2008). To assess functional reorganization in the sensorimotor system, we devised a functional MRI protocol that entailed a motor task and sensory stimulation for group comparisons of task-related activation. We then tested whether trauma-induced spinal changes were associated with altered task-related blood oxygenation level-dependent (BOLD) signal and whether both brain and spinal cord structural changes and brain functional changes were associated with disability.

Materials and methods

Subjects

Ten right-handed male subjects [mean (SD) age 47.1 (10.7) years, range 29–61 years], with cervical SCI, who fulfilled the following inclusion criteria, were recruited: (i) upper and lower limb impairment; (ii) no head or brain lesion associated with the trauma leading to the injury; (iii) no seizure, no medical or mental illness; and (iv) no MRI contraindications.

Sixteen right-handed (right-dominant) control subjects, with a mean (SD) age of 39.3 (15.4) years, range 25–71 years) were recruited. The mean ages of the control and SCI group were not significantly different.

All subjects gave informed, written consent before the study, which was approved by the Joint Ethics Committee of the Institute of Neurology and the National Hospital of Neurology and Neurosurgery (ref: 08/0243).

In all participants, bilateral upper limb function was assessed on the day of scanning using the 9-Hole Peg Test and the maximum voluntary contraction of the dominant hand. In subjects with SCI, the Action Research Arm Test (ARAT) of the dominant hand was also used (Lyle, 1981). Three subjects with SCI were unable to perform the 9-Hole Peg Test with their non-dominant hand and were scored with the maximum time allowed for the 9-Hole Peg Test (300 s) (Hoogervorst *et al*., 2002). The average of two trials of the 9-Hole Peg Test was calculated for each hand. For comparison of clinical measures of upper limb function between subjects with SCI and controls, the Mann–Whitney U-test was used (Statistical Package for the Social Sciences-17.0; SPSS Inc.) and results at a significance level of $P < 0.05$ were reported.

Image acquisition, post-processing and statistical analysis

Subjects were scanned on a 1.5 T whole-body Magnetom Sonata MRI scanner (Siemens Healthcare) operated with a radio frequency body transmit and an eight-channel receive head coil.

Anatomical imaging of the brain and spinal cord

A 3D whole-brain, structural scan including brainstem and cervical cord (down to C5) was acquired using a T_1-weighted modified driven equilibrium Fourier transform (MDEFT) sequence, optimized for simultaneous assessment of the brain and spinal cord (Deichmann *et al*., 2004; Freund *et al*., 2010). The imaging parameters were: isotropic 1 mm^3 resolution, field of view 256 × 256 mm^2, matrix 256 × 256, 176 sagittal partitions, repetition time = 12.24 ms, echo time = 3.56 ms, inversion time = 530 ms, flip angle 23°, fat saturation, bandwidth 106 Hz/pixel and a scan time of ~13 min 43 s. All images were checked for movement artefacts.

Cord atrophy

Cross-sectional cord area was measured on a series of five contiguous axially reformatted slices (3-mm slice thickness) derived from the T_1-weighted volume using a well-established semi-automated segmentation method (Losseff *et al*., 1996; Freund *et al*., 2010). The Mann–Whitney U-test was used to evaluate the cord area difference between subjects with SCI and controls. To test for an association between impairment and cross-sectional cord area in subjects with SCI, we used multiple linear regression analysis, with the behavioural measure as the dependent variable and cord area as an independent variable, together with height, weight and age. The normality of the residuals of the regression was ascertained by inspection of the Q–Q plots. $P < 0.05$ was considered significant.

Voxel-based morphometry

We applied VBM as implemented in Statistical Parametric Mapping-8 (http://www.fil.ion.ucl.ac.uk/spm) to perform voxel-wise comparisons of grey and white matter volume between the two groups of subjects (Ashburner *et al*., 2003). First, a unified model inversion (unified segmentation) (Ashburner *et al*., 2003) was used for bias correction and segmentation of 3D T_1-weighted MDEFT images into grey matter, white matter and CSF. A diffeomorphic non-linear image registration tool (Diffeomorphic Anatomical Registration using Exponentiated Lie algebra (DARTEL)) (Ashburner, 2007), was used to warp the grey matter and white matter segments into an optimal (average) space. The resulting grey matter and white matter images were modulated and affine transformed to Montreal Neurological Institute space and smoothed using an isotropic Gaussian kernel with 6 mm full width at half-maximum.

Voxel-based cortical thickness

From the grey matter, white matter and CSF segments (created in the preprocessing step of the VBM analysis) a VBCT map was created (Hutton *et al*., 2009). The input tissue segments were sub-sampled from 1 mm to 0.5 mm using trilinear interpolation to increase resolution for narrow CSF spaces. VBCT maps were computed by extracting the cortical grey matter boundaries and estimating the distance between the inner and outer grey matter boundaries at each voxel in the cortex (Hutton *et al*., 2008). The resulting VBCT maps contain a value for cortical thickness at each voxel in grey matter and zeros elsewhere. VBCT maps were then warped into the same reference space as the grey matter probability maps and smoothed using an isotropic 6-mm full width at half-maximum Gaussian kernel with a correction to preserve local cortical thickness (Hutton *et al*., 2009).

Statistical analysis of voxel-based morphometry and voxel-based cortical thickness

Statistical analysis of the processed imaging data was performed using the general linear model and the theory of Gaussian random fields (Friston *et al*., 1995*b*). Group comparisons were performed by means of a Statistical Parametric Mapping analysis of covariance (ANCOVA) using the total volume of each segmented image (grey matter volume for grey matter analysis, white matter volume for white matter analysis) and the cortical thickness values of the VBCT maps as a covariate of interest. Differences between groups were assessed by using two-sample, two-tailed *t*-tests at each voxel. Age and total intracranial volume (i.e. CSF + white matter + grey matter) were included as (nuisance) covariates of no interest to exclude possible effects on regional grey matter and white matter volumes and cortical thickness differences.

Region of interest analysis of grey matter and white matter volume and cortical thickness

A whole-brain analysis was conducted to provide an unbiased (data-led) overview of effects. In addition, (hypothesis-led) searches for significant effects were restricted to *a priori* regions of interest corresponding to primary motor cortex and primary sensory leg and hand areas, and white matter regions along the corticospinal tract, to maximize sensitivity at a threshold of $P < 0.05$ (corrected for multiple comparison within region of interest). For the VBM and VBCT analysis, a 10-mm sphere was centred on $x = -6$, $y = -28$, $z = 60$ for primary motor cortex leg area (from Ciccarelli *et al*., 2005), on $x = -42$, $y = -18$, $z = 58$ for primary motor cortex hand area (from Talelli *et al*., 2008), and on $x = -4$, $y = -46$, $z = 62$ (from Ferretti *et al*., 2003) for primary sensory cortex leg area, in the Montreal Neurological Institute coordinate system. For white matter VBM, we extracted from the ICBM-DTI-81 white matter labels atlas (Mori *et al*., 2008): left and right pyramids, cerebellar peduncle and posterior limb of the internal capsule.

After characterizing the average group effects, we tested for the regional structural correlates of upper limb function in the same regions of interest. We performed a voxel-wise linear regression analysis in Statistical Parametric Mapping-8 in subjects with SCI. Each linear regression model comprised one of the clinical parameters of interest (9-Hole Peg Test, maximum voluntary contraction, ARAT, American Spinal Injury Associations score) with age and total intracranial volume as two nuisance covariates. Statistical parametric *t*-maps report linear increases or decreases in grey matter volume that can be explained by the clinical parameter (that cannot be explained by the confounding effects modelled by the nuisance variables). The *t*-tests were two-tailed and the associated *P*-values were corrected for multiple comparisons within *a priori* defined regions of interest ($P < 0.05$) using Gaussian random field theory (Friston *et al*., 1995*b*).

Functional imaging of the brain

BOLD sensitive functional MRI was carried out using a single-shot, gradient echo, echo-planar imaging sequence (echo time = 50 ms, repetition time = 4.3 s, flip angle $\alpha = 90°$, field of view 192 × 192 mm^2, acquisition matrix 64 × 64, readout bandwidth (BW) = 2298 Hz/pixel, voxel size 3 × 3 × 2 mm) on the same day of the acquisition of the T_1-weighted MDEFT images. Each data volume comprised 48 axial slices of 2 mm thickness, with 1 mm inter-slice gap, acquired in descending order.

Functional magnetic resonance imaging paradigm

All stimuli were controlled using the Matlab 7 (The Mathworks Inc.) toolbox Cogent 2000 (http://www.vislab.ucl.ac.uk/Cogent/) running on a conventional PC. The functional MRI task consisted of active 20 s blocks of right sided: (i) repetitive isometric handgrip; (ii) electrical

median nerve stimulation at the medial wrist; or (iii) electrical tibial nerve stimulation at the medial malleolus. Six repetitions of the 20 s blocks were performed alternating with 20 s rest blocks (starting with a rest block). The active blocks were presented in pseudo-randomized order.

All participants lay supine and viewed visual stimuli projected onto a frosted screen via a mirror system mounted above the magnetic resonance head-coil. A centrally presented visual columnar display (in form of a thermometer) gave visual feedback about the amount of force subjects were exerting and indicated the 30% maximum voluntary contraction level. Handgrips were performed using an MRI compatible grip manipulandum as described previously (Ward and Frackowiak, 2003). Prior to scanning, but while supine in the scanner, subjects were asked to grip the manipulandum twice, using maximum force to generate a maximum voluntary contraction for the grip hand (maximum strength signal was represented by height or amplitude in millivolts). The target force of 30% of maximum voluntary contraction was derived for each subject from the maximum of two trials prior to scanning. Subjects were instructed to maintain a (30% maximum voluntary contraction) handgrip for the duration of a visual cue (1.7 s) during task blocks. All subjects practiced the motor task (~20 times) until comfortable. In total, 48 (eight per block) handgrips were performed during data acquisition.

For electrical stimulation of the median and tibial nerve, a pair of surface-adhesive electrodes was positioned on the right medial wrist and the right medial malleolus. Stimuli were electrical rectangular pulses, 0.2 ms in duration, with a repetition rate of 4 Hz using a battery-powered neurostimulator (DS7A, Digitimer) located within a shielded box inside the scanner room (to preclude magnetic resonance artefacts and for safety reasons). Stimulation intensities were adjusted to a painless motor threshold producing a visible thumb opposition or toe flexion. Eighty stimuli were delivered per block and nerve, giving 480 stimuli per stimulation site. During the functional MRI experiment one of the investigators carefully monitored the subjects with SCI to ensure there were no time-locked movements in the lower extremity in response to handgrip or median nerve stimulation. However, this does not exclude the possibility of subtle co-contractions of leg muscles (e.g. contraction of the extensor hallucis), as we did not control for this confound using electromyography recordings.

Functional magnetic resonance imaging post-processing and statistical analysis

Two subjects with SCI were unable to complete the functional MRI scan because of technical problems related to the stimulation equipment and were therefore excluded from further analysis. Functional MRI data quality was monitored online (Weiskopf *et al*., 2007). The ensuing images were reconstructed offline using a trajectory-based image reconstruction (Josephs *et al*., 2000) and analysed using Statistical Parametric Mapping-5. A total of 166 image volumes was acquired from each subject. The first six image volumes were discarded to allow for T_1 equilibration effects. The remaining volumes were realigned to the first, unwarped to account for movement-induced image distortions (Andersson *et al*., 2001), slice-time corrected, normalized to the Montreal Neurological Institute anatomical standard space, and smoothed spatially with an isotropic 8-mm full width at half-maximum Gaussian kernel. Translatory motion was <2.5 mm in all subjects.

The functional MRI time series from each subject was analysed separately using a general linear model comprising box-car stimulus functions encoding the three block conditions (Friston *et al*., 1995*a*, *b*) convolved with a canonical haemodynamic response function. Temporal derivates of the canonical haemodynamic response function were also included in the first (within-subject)-level analysis to accommodate latency and slice-timing effects. The first-level analysis produced subject-specific contrast images where each value represented the activations in the handgrip, median or tibial stimulation condition compared with the rest condition. The contrast images were then used in a second (between-subject)-level two-sample *t*-test to identify abnormal activation in regions of interest in subjects with SCI relative to controls. Age was included in the second-level model and treated as a covariate of no interest.

To test for influence of trauma-induced spinal changes (i.e. cord area) and upper limb function on task-related activation, we then used voxel-wise linear regression analyses that were formally identical to the analysis of the structural data: each regression model comprised either cord area or a clinical parameter of interest and age as a nuisance covariate. Statistical parametric maps were computed showing where a linear increase or decrease in activation could be explained by the parameter of interest. The *t*-tests were one-tailed and the associated *P*-values were corrected for multiple comparisons using Gaussian random field theory (Friston *et al*., 1995*b*). Searches for significant effects were restricted to *a priori* regions of interest (below) to maximize sensitivity at a threshold of $P < 0.05$ corrected for multiple comparison within the region of interest.

To ensure that the sensitivity of functional MRI was the same across the two groups, the temporal signal-to-noise ratio was measured in the sensorimotor cortex in each subject by dividing the signal mean by the square root of the sum of the squares of the model residuals. Averaging these values over each group resulted in temporal signal-to-noise ratio = 171.61 (SEM 7.67) for the subjects with SCI and 179.12 (SEM 4.81) for the controls. This indicates a negligible difference in temporal signal-to-noise ratio and sensitivity ($P = 0.39$, *t*-test).

Regions of interest for functional MRI analysis

The Statistical Parametric Mapping Anatomy toolbox (http://www.fz-juelich.de/inm/inm-1/spm_anatomy_toolbox) was used to specify search volumes in primary motor cortex, primary sensory cortex and secondary sensory and premotor cortex in both hemispheres, as our hypothesis was restricted to the sensorimotor system. The *a priori* regions of interest for activation effects in subjects with SCI were the left primary motor cortex, left dorsal premotor cortex and left rostral and caudal ventrolateral premotor cortex for the handgrip. The regions of interest were defined as 10 mm spheres centred on peak coordinates of task-related activation derived from Ciccarelli *et al*. (2005): primary motor cortex leg region ($x = -6$, $y = -28$, $z = 60$); and from Ward and Frackowiak (2003): dorsal premotor cortex ($x = -24$, $y = -12$, $z = 66$), caudal ventral premotor cortex ($x = -54$, $y = -6$, $z = 6$) and rostral ventral premotor cortex ($x = -56$, $y = 6$, $z = 14$). For task-related activations during peripheral nerve stimulation the regions of interest consisted of Brodmann area (BA) 3a and BA 3b as defined by the Anatomy toolbox implemented in Statistical Parametric Mapping-8.

Results

Clinical data

Ten subjects with SCI had lesions of the cervical cord between C5 C8 (Table 1). Eight had incomplete and two a complete lesion

Table 1 Individual clinical and behavioural data for the subjects with SCI with means

Subject with SCI	Age (years)	Aetiology of the injury	Time since injury (years)	Level of motor impairment/ ASIA	Upper limb motor score	Lower limb motor score	Dominant hand 9HPT	Non-dominant hand 9HPT	MVC	ARAT	Light touch	Pinprick
1	43	Fracture	14	C6/D	25	30.5	68	54.35	0.22	36	44.50	68
2	29	Fracture	9	C6/B	19	0	52.6	59.2	0.05	42	24.50	52.6
3	44	Fracture	7	C7/C	14	19	56.75	118.4	0.25	57	88.00	56.75
4	35	Fracture	14	C5/A	18.5	0	190.5	300	0.02	26	66.50	190.5
5	60	Spinal stenosis	12	C6/C	46.5	19	26.25	24.55	0.47	57	102.50	26.25
6	61	Fracture	19	C6/A	34	0	68.3	76.5	0.05	26.5	16.00	68.3
7	40	Disc prolapse	19	C5/C	20.5	18.5	283	300	0.01	26	66.50	283
8	53	Fracture	7	C8/D	43.3	48	38.55	42.45	0.25	53	29.00	38.55
9	56	Fracture	15	C5/D	23.5	34.5	105	300	0.11	25	85.50	105
10	50	Fracture	30	C5/D	25	22	20.1	21.8	0.22	57	112	104
Median					24.25	19.00	62.37	67.85	0.16	39.00	96.25	66.50
IR					17.45	31.50	90.90	262.03	0.21	31.25	33.88	92.00
Controls												
Median							16.92	17.80	0.57			
IR							2.35	2.65	0.36			

ASIA = American Spinal Injury Association impairment scale; 9HPT = 9-Hole Peg Test; MVC = maximum voluntary contraction.

based on the American Spinal Injury Associations impairment classification. The mean (SD) period post-SCI was 14.6 (6.91) years (range 7–30 years). Subjects with SCI had reduced American Spinal Injury Associations motor and sensory scores of upper and lower limb and were impaired on the ARAT (median score of 39 of max 57) (Table 1). Subjects with SCI were impaired on the dominant hand, as assessed by the 9-Hole Peg Test {subjects with SCI: median [interquartile range (IR)] 62.37 (90.90) s versus controls: median (IR) 16.92 (2.35) s; Mann–Whitney $U = 160$, $z = -4.217$ $n_c = 16$, $n_p = 10$, $P < 0.001$}, on the non-dominant hand, as assessed by the 9-Hole Peg Test [subjects with SCI: median (IR) 67.85 (262.03) s versus controls: median (IR) 17.8 (2.65) s; Mann–Whitney $U = 159$, $z = 4.163$ $n_c = 16$, $n_p = 10$, $P < 0.001$] and the maximum voluntary contraction [subjects with SCI: median (IR) 0.16 (0.21) mV versus controls: median (IR) 0.57 (0.36) mV; Mann–Whitney $U = 146$, $z = 3.478$ $n_c = 16$, $n_p = 10$, $P < 0.001$] compared with controls (Table 1). Subjects with SCI also experienced reduced regional tactile sensitivity in the upper limb, as assessed by light touch and pin prick score (Table 1).

Spinal cord atrophy and brain white matter and grey matter changes

Subjects with SCI had reduced cord area compared with controls [subjects with SCI: median (IR) 54.85 (12.42) mm^2 versus controls: median (IR) 77.6 (11.3) mm^2; Mann–Whitney $U = 160$, $z = -4.217$ $n_c = 16$, $n_p = 10$, $P < 0.001$] (Fig. 1).

VBM analysis revealed smaller regional white matter and grey matter volume in subjects with SCI compared with controls (Supplementary Table 1). In particular, smaller white matter volume was detected in the bilateral pyramids ($P \leqslant 0.002$, corrected for multiple comparisons within region of interest) and left cerebellar peduncle ($P = 0.017$, corrected for multiple comparisons within region of interest) (Fig. 2A) and lower grey matter volume in the leg area of right primary motor cortex ($P = 0.005$, corrected for multiple comparisons within region of interest) (Fig. 2B). This cluster extended in a rostral–caudal direction from $y = -29$ to -43, in the ventral–dorsal direction from $z = 57$–70 and into both hemispheres from $x = -2$ to 11, thus additionally encompassing left primary motor cortex and right primary sensory cortex.

VBCT analysis revealed decreased cortical thickness in the leg area of primary sensory cortex adjacent to and extending beyond the region identified by VBM in subjects with SCI compared with controls ($P = 0.012$, corrected for multiple comparisons within region of interest) (Fig. 2B, Supplementary Table 1).

Subjects with SCI showed no increased regional white matter or grey matter volume or greater cortical thickness in any regions of interest when compared with controls.

Association of spinal and cortical atrophy with upper limb impairment

In subjects with SCI, greater cord area was associated with: (i) better dominant hand 9-Hole Peg Test performance [$P = 0.002$, coefficient of variation (coeff.) = -9.807, 95% confidence interval (CI) -14.67 to -4.94]; (ii) non-dominant hand 9-Hole Peg Test ($P = 0.011$, coeff. = -12.669, 95% CI -21.49 to -3.85); and (iii) ARAT ($P = 0.039$, coeff. = 1.302, 95% CI 0.088–2.517) (Fig. 3).

In subjects with SCI, grey matter volume in the leg area of primary motor cortex correlated positively with maximum voluntary contraction ($P = 0.014$, corrected for multiple comparisons within region of interest) and dominant hand 9-Hole Peg Test ($P = 0.001$, corrected for multiple comparisons within the region of interest) (Fig. 4A and B, Table 2).

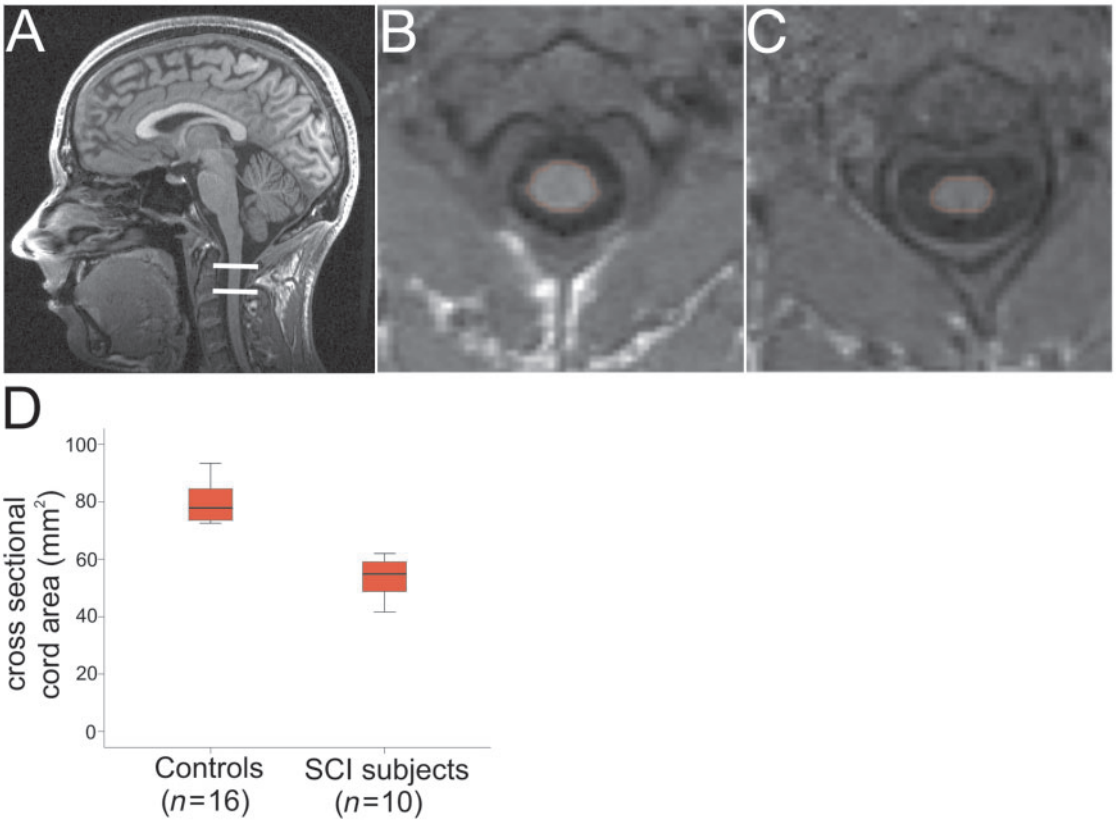

Figure 1 Spinal cord atrophy following SCI. (**A**) T_1-weighted scan of the brain and cervical spinal cord showing the region of cross-sectional cord area measurement (within white horizontal bars). (**B** and **C**) Cord area in a control and subject with SCI, respectively. (**D**) Box and whisker plots showing a 30% reduction in cord area in subjects with SCI compared with controls.

Figure 2 Statistical parametric maps (thresholded at $P < 0.001$, uncorrected for display purposes only) showing regions of white matter and grey matter volume reduction in subjects with SCI compared with controls. (**A**) Smaller white matter volume in the pyramids and the left cerebellar peduncle and (**B**) smaller grey matter volume (yellow) and reduced cortical thickness (red) in the leg area of primary motor cortex and primary sensory cortex. Note, the overlap (orange) and the different areas detected with VBCT in addition to the VBM analysis.

Functional changes and their association with cord area and upper limb impairment

There were significant differences in functional MRI activation during handgrip and median nerve stimulation (i.e. task versus rest) between subjects with SCI and controls, and significant correlations between cord area and upper sensory function with task-related activations as explained below.

Handgrip

Subjects with SCI exhibited relative increases in task-related BOLD signal in left superior, medial precentral gyrus consistent with the leg representation within primary motor cortex compared with controls ($P = 0.006$, corrected for multiple comparisons within

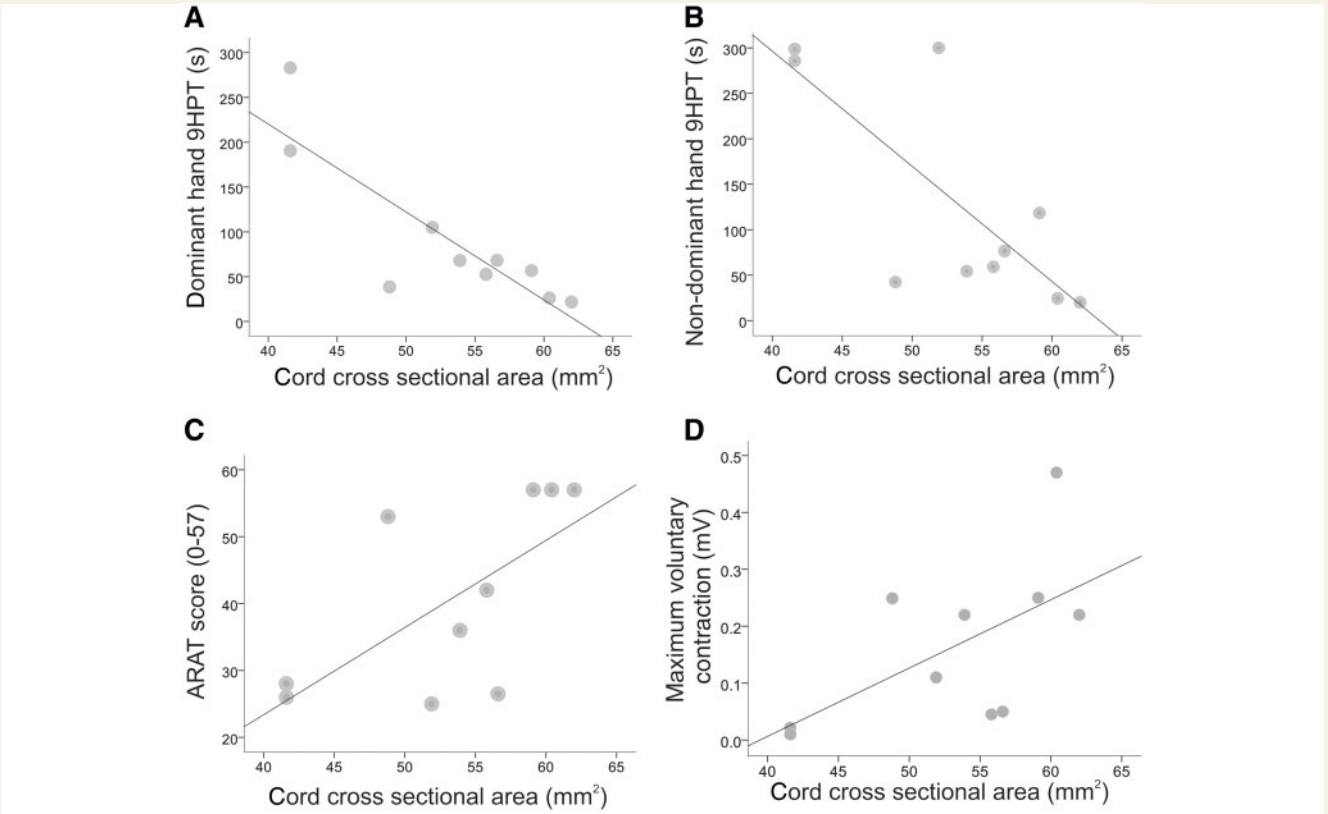

Figure 3 Graphs showing significant correlations between clinical measures of upper limb function and lower cord area (cross sectional) in subjects with SCI. (**A**) Dominant hand 9-Hole Peg Test and cord area; (**B**) Non-dominant hand 9-Hole Peg Test and cord area; (**C**) ARAT and cord area; and (**D**) Maximum voluntary contraction and cord area.

region of interest) (Fig. 5A, Supplementary Table 2). Linear regression analyses revealed an association between lower cord area and greater task-related BOLD signal during right handgrip in the leg area of primary motor cortex ($P = 0.005$, corrected for multiple comparisons within region of interest) (Fig. 6A, Table 3). In other words, task-related brain activation was greater in left primary motor cortex (leg) in subjects with SCI with greater cord damage.

Median nerve stimulation

Task-related activation during right median nerve stimulation was greater for subjects with SCI compared with controls in a more inferior part of left primary sensory cortex (corresponding to the face area) (Curt *et al*., 2002) (Fig. 5B). Linear regression analyses revealed a negative correlation between cord area and brain activation during right median nerve stimulation, again in the face area of primary sensory cortex ($P = 0.031$, corrected for multiple comparisons within region of interest) (Fig. 6B, Supplementary Table 2). Moreover, increases in task-related BOLD signal during median nerve stimulation in primary sensory cortex was correlated with lower light touch score ($P < 0.05$, corrected for multiple comparisons within region of interest) (Fig. 7A and B, Table 4) and lower pinprick score ($P < 0.001$, corrected for multiple comparisons within region of interest) (Fig. 7C, Table 4) in subjects with SCI. In other words, subjects with SCI with greater cord damage and greater reduction in tactile sensitivity showed greater brain activation of the face area of left primary sensory cortex during right median nerve stimulation.

Tibial nerve stimulation

Subjects with SCI did not show any activation increases in BOLD signal during tibial nerve stimulation relative to control. However, greater cord area correlated with increased BOLD signal during tibial nerve stimulation in the leg area of primary sensory cortex ($P = 0.046$, corrected for multiple comparisons within region of interest) (Fig. 6C, Table 3). In other words, cord area was positively associated with activation in the leg representing area of primary sensory cortex.

There were no increases in task-related BOLD signal in controls when compared with subjects with SCI.

Discussion

In this study we have focused on trauma-induced structural and functional changes in the brain, and structural changes in the cervical cord. In particular, we have considered the relationship between the two and their impact on disability.

Subjects with SCI had a reduction of 30% of cord area compared with controls. Spinal cord atrophy represents the endpoint

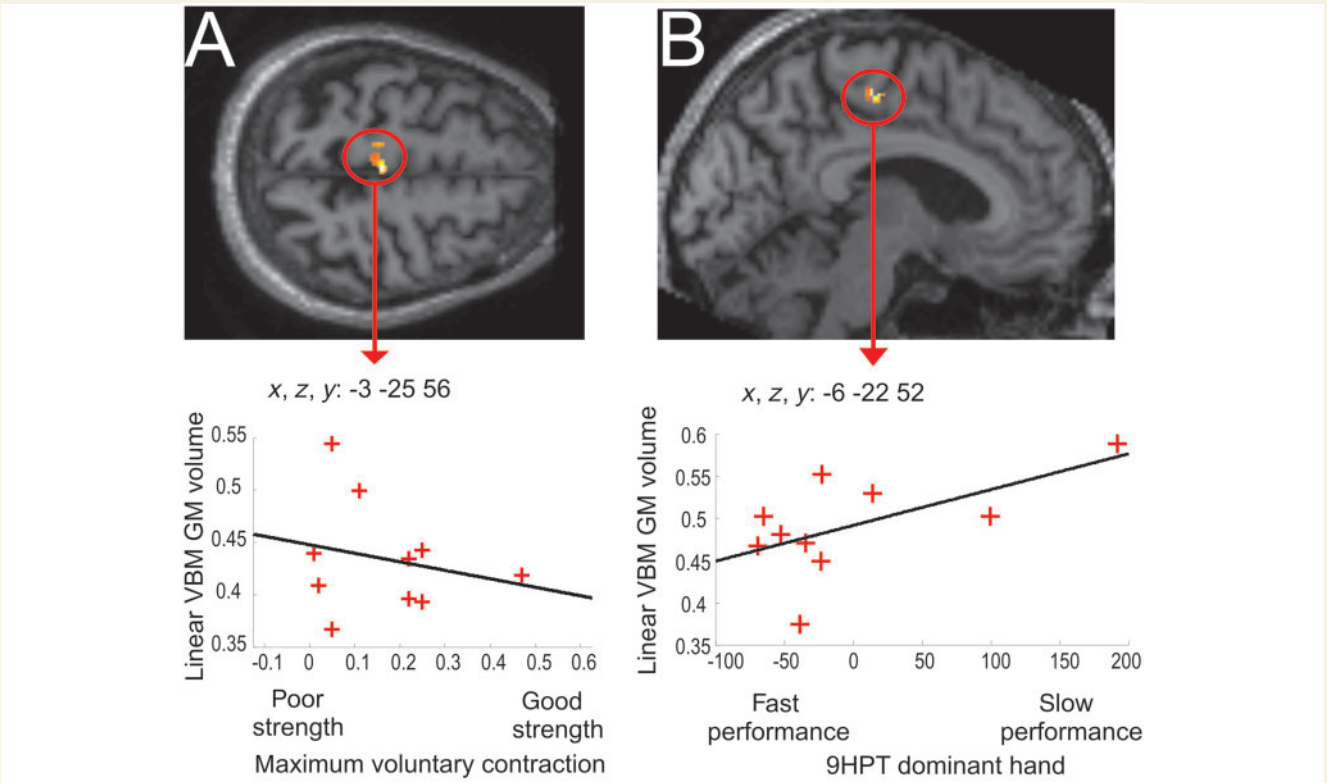

Figure 4 Statistical parametric maps showing the results of the regression analyses of clinical measures of upper limb function and grey matter volume in subjects with SCI. (**A**) Region of increased grey matter volume in left leg area of primary motor cortex associated with lower grip strength (maximum voluntary contraction) of the dominant hand ($P = 0.014$, corrected for multiple comparisons within region of interest). (**B**) Region of increased grey matter volume and slower performance of the 9-Hole Peg Test (9HPT) of the dominant hand ($P = 0.001$, corrected for multiple comparisons within region of interest). Note that scatter plots are depicted for illustrative purposes showing the associations between the grey matter volume of each individual subjects with SCI plotted against the upper limb motor performance from each subject with SCI. Improved motor function corresponds to higher values for maximum voluntary contraction and lower values for 9-Hole Peg Test (along the *x*-axis). GM = grey matter.

Table 2 Grey matter volume associations with upper limb function in subjects with SCI

Region	Coordinates in MNI space				
	Side	x	y	z	Z-value
Negative correlation between grey matter volume and MVC					
Primary motor cortex (BA 4a) leg area	L	−3	−25	55	4.07
Negative correlation between grey matter volume and dominant hand 9HPT					
Primary motor cortex (BA 4a) leg area	L	−6	−22	52	4.66

Brain voxels of *a priori* regions of interest are significant at $P < 0.05$, corrected for multiple comparisons. 9HPT = 9-Hole Peg Test; MNI = Montreal Neurological Institute; MVC = maximum voluntary contraction; L = left.

of neurodegeneration resulting from an accumulation of multiple pathophysiological events, such as axonal degeneration and demyelination, axonal dieback and neuronal loss (Dusart and Schwab, 1994). Given that animal models of SCI have demonstrated only limited axonal regeneration (Freund *et al*., 2006), treatment-induced psychometric change of motor and sensory function in humans may be minimal. However, the American Spinal Injury Associations standard of clinical assessment lacks the sensitivity to delineate minimal change in psychometric properties of motor and sensory function (Ellaway *et al*., 2010). To overcome this shortcoming, we focused on clinical measures of hand function. Crucially, lower atrophy of the cervical cord correlated with better hand function, as measured by the 9-Hole Peg Test, maximum voluntary contraction and ARAT. Thus, we demonstrate clinically eloquent relationships, which speak to future assessments in longitudinal studies, and further validate

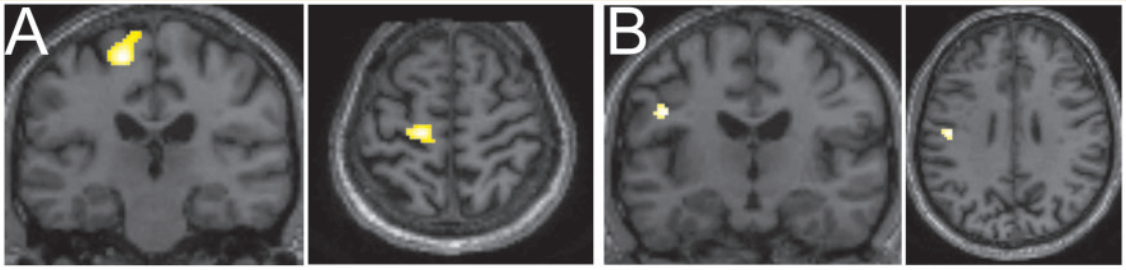

Figure 5 Statistical parametric maps (thresholded at $P < 0.001$, uncorrected for display purposes only) showing regions of increased task-related brain activity in subjects with SCI compared with controls. (**A**) Increased BOLD response during right-sided handgrip in contralateral left leg area of primary motor cortex and (**B**) during right-sided median nerve stimulation in contralateral left face area of primary sensory cortex.

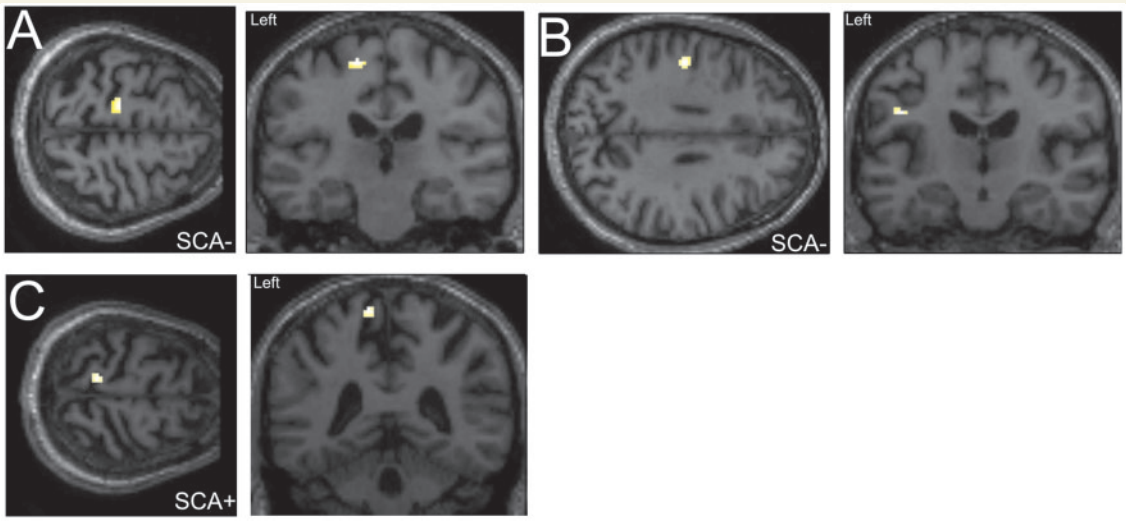

Figure 6 Statistical parametric maps (thresholded at $P < 0.001$, uncorrected for display purposes only) showing negative associations between cord area and (**A**) increased task-related BOLD signal in the left leg area of primary motor cortex during right-sided handgrip and (**B**) in the left face area of primary sensory cortex during right-sided median nerve stimulation. (**C**) Cord area was positively associated with normal task-related BOLD signal in the leg area of primary sensory cortex during tibial nerve stimulation. SCA = cord cross sectional area.

Table 3 Influences of spinal cord atrophy on task-related BOLD activation

Region	Coordinates in MNI space				
	Hemisphere	*x*	*y*	*z*	Z-value
Activation during handgrip correlates negatively with cord area					
Primary motor cortex (BA 4a, leg area)	Contralateral	−14	−24	58	3.96
Activation during median nerve stimulation correlates negatively with cord area					
Primary sensory cortex (BA 3a)	Contralateral	−46	−18	30	3.74
Activation during tibial nerve stimulation correlates positively with cord area					
Primary sensory cortex (BA 3a)	Contralateral	−12	−42	66	3.54

All brain voxels are significant at $P < 0.05$, corrected for multiple comparisons within *a priori* region of interest of the sensorimotor cortex.

clinical measures of upper limb function and American Spinal Injury Associations scores, in relation to spinal atrophy (Lundell *et al*., 2010*a*).

Using VBM, we found a reduction of regional white matter volume in both pyramids and the left cerebellar peduncle of the corticospinal tract. We demonstrated cortical grey matter atrophy in 'paralyzed' regions of primary motor cortex and primary sensory cortex, in agreement with previous reports (Jurkiewicz *et al*., 2006; Wrigley *et al*., 2009*a*). In addition, we showed decreased cortical thickness (as detected by VBCT) adjacent to, and beyond

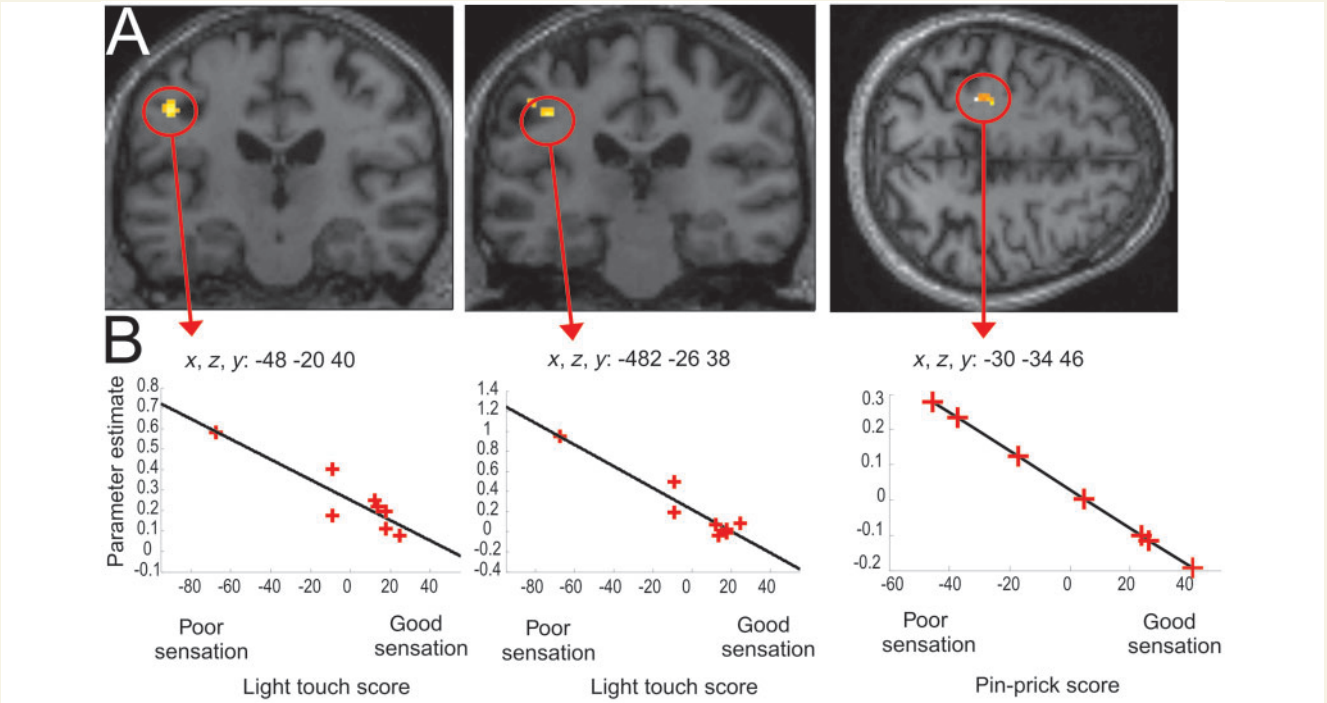

Figure 7 Sensory deficits are associated with increased BOLD signal in primary sensory cortex. (**A**) Statistical parametric maps (thresholded at $P < 0.001$, uncorrected for display purposes only) showing associations between task-related brain activity and sensory deficits in subjects with SCI in primary sensory cortex. (**B**) Parameter estimates from each individual subject with SCI for the main effect of median nerve stimulation plotted against light touch and pinprick score from each subject with SCI (along the *x*-axis) for the circled regions in **A**.

Table 4 Sensory correlates during median nerve stimulation in primary sensory cortex

Coordinates in MNI space					
Region	**Side**	***x***	***y***	***z***	**Z-value**
Correlation between task related BOLD signal during median nerve stimulation and light touch score					
Primary sensory cortex/BA 3b	C	−48	−20	40	3.63
Primary sensory cortex/BA 3a	C	−42	−26	38	3.61
Correlation between task related BOLD signal during median nerve stimulation and pinprick score					
Primary sensory cortex/BA 3a	C	−30	−34	46	4.35

All brain voxels are significant at $P < 0.05$, corrected for multiple comparisons within *a priori* region of interest of the primary sensory cortex. C = contralateral; MNI = Montreal Neurological Institute.

that, detected by VBM. VBCT measures cortical thinning, while VBM measures grey matter volume changes that include changes in cortical surface area and thickness (Ashburner and Friston, 2000; Hutton *et al*., 2009). We did not detect any volumetric decreases in other brain areas such as the prefrontal cortex (Wrigley *et al*., 2009*a*), although this might be due to our sample size that may have low power for weak effects.

Overall, the reduction of subcortical white matter volume in the corticospinal tract and cortical grey matter volume and cortical thinning in primary motor cortex is indicative of atrophy due to retrograde degeneration (Hains *et al*., 2003; Beaud *et al*., 2008), but could also arise from decreased cortical connectivity due to a reduction in dendritic spine density (Kim *et al*., 2006) or a reduction in angiogenesis (Fields, 2008). Atrophy of neurons in primary sensory cortex may be induced through reduced cellular activity, triggered by transneuronal degeneration (Jones, 2000). CNS atrophy and its relationship with clinical impairment may prove to be a pathologically specific marker in clinical trials of spinal cord repair, as brain volume change has been used as an outcome measure in trials in patients with multiple sclerosis (Barkhof *et al*., 2010).

Based on functional and anatomical assessment, we were able to show: (i) relative increases in task-related brain activity during right handgrip in the left leg area of primary motor cortex; (ii) that spinal atrophy predicted activation differences; and (iii) structural associations between measures of upper limb function and grey matter volume in the 'paralyzed' leg region of left primary motor cortex. Despite many studies demonstrating cortical reorganization after human SCI (for review see Kokotilo *et al*., 2009), there is no

consensus about the role of output-deprived corticospinal neurons. Findings range from an expansion of task-related brain activation (Curt *et al*., 2002; Jurkiewicz *et al*., 2007) that is related to atrophy of the lateral part of the cervical cord (Lundell *et al*., 2010*b*) to unaltered brain activity during a similar upper limb task (Shoham *et al*., 2001; Turner *et al*., 2003) and reduced brain activation of subjects with SCI with persistent paralysis (Jurkiewicz *et al*., 2010). The expansion of the cortical primary motor cortex hand area into the output-deprived primary motor cortex leg area, as observed in the present study, may be related to rewiring of axotomized hind limb neurons onto cervical motor circuits (Ghosh *et al*., 2010), driven by compensatory use of a less affected part of the body, similar to that seen following rehabilitative training after stroke (Nudo *et al*., 1996) or overuse (Elbert *et al*., 1995). However, as subjects with better upper limb function did not show an increased grey matter volume in the primary motor cortex leg area, an alternative interpretation could be that greater disability induces greater cortical reorganization but that this does not translate into functional gain. Furthermore, increased cortical activation could also be attributed to an inter-limb coupling that can occur following severe cervical SCI (i.e. upper limb movements are associated with automatically occurring lower limb movements) (Calancie *et al*., 1996). Although we did not observe any time-locked leg muscle movements during the handgrip task, this does not exclude the possibility of subtle co-contractions (for example, of the extensor hallucis), which could contribute to the activation in the primary motor cortex leg area. Finally, we are confident that the relative increases in task-related BOLD signal cannot be explained by performance confounds, because we asked participants to exert 30% of their maximum voluntary contraction during the handgrip task and used a subject-specific (non-painful) threshold during peripheral nerve stimulation.

Within primary sensory cortex, we show an increase in task-related BOLD signal in the face area during median nerve stimulation in subjects with SCI, compared with controls. This finding is in general agreement with previous reports in subjects with SCI with neuropathic pain (Wrigley *et al*., 2009*b*) and referred phantom sensation (Moore *et al*., 2000). Importantly, the spread in task-related BOLD signal into the face area of primary sensory cortex is predicted by spinal atrophy and relates quantitatively to sensory deficits in subjects with SCI. These findings suggest that greater damage to the spinal cord induces greater cortical reorganization that relates quantitatively to disability. Cortical and subcortical mechanisms that underlie this reorganization of primary sensory cortex are not well understood. On the one hand, it might be driven by an overall reduction of grey matter volume in primary sensory cortex, which is known to correlate with sensory deficits (Jurkiewicz *et al*., 2006), but could also arise from afferent volleys induced by median nerve stimulation to the trigeminal nuclei (Jain *et al*., 2000).

As expected, stimulation below the injury site (i.e. tibial nerve) did not elicit robust task-related activation. Voxel-wise regression analysis indicated that absence of task-related brain activity during tibial nerve stimulation might be due to spinal atrophy. Put simply, cord atrophy might preclude information flow towards the cerebrum. Thus, by applying peripheral nerve stimulation to nerves of the lower and the upper extremities allows for the differential investigation of long sensory fibre tracts innervating the upper versus lower extremities.

In conclusion, we show that traumatic SCI leads to spinal and cortical atrophy. Cortical changes in functional MRI indicate shifts of functional motor and sensory representations that relate to the severity of spinal damage. Clinical impairment is predicted by non-invasive imaging of spinal atrophy and cortical reorganization, in particular, cervical cord area, BOLD signal and grey matter volume in primary motor cortex leg area, and BOLD signal in primary sensory cortex face area. We consider these imaging parameters as potential biomarkers for future clinical trials looking at repair of the injured spinal cord and thus call for further assessment in longitudinal studies of SCI.

Acknowledgements

We thank all participants who participated in this study, Judith Susser and Dr Vernie Balasubramaniam, Eric Featherstone and the team of the radiographers of the Wellcome Trust Centre for Neuroimaging, for technical support. We would also like to thank Dr Daniel Altman for statistical advice and Prof. Roger Lemon for critical review of a former version of this manuscript.

Funding

Swiss National Science Foundation (grant no. PBFR33-120920); Schweizerische Stiftung für medizinische und biologische Stipendien (grant no. PASMP3-124194); Swiss Paraplegic Research (Nottwil); Wellcome Trust. This work was undertaken at UCLH/UCL who received a proportion of funding from the Department of Health's NIHR Biomedical Research Centres funding scheme.

Supplementary material

Supplementary material is available at *Brain* online.

References

Andersson JL, Hutton C, Ashburner J, Turner R, Friston K. Modeling geometric deformations in EPI time series. Neuroimage 2001; 13: 903–19.

Ashburner J. A fast diffeomorphic image registration algorithm. Neuroimage 2007; 38: 95–113.

Ashburner J, Csernansky JG, Davatzikos C, Fox NC, Frisoni GB, Thompson PM. Computer-assisted imaging to assess brain structure in healthy and diseased brains. Lancet Neurol 2003; 2: 79–88.

Ashburner J, Friston KJ. Voxel-based morphometry–the methods. Neuroimage 2000; 11: 805–21.

Bareyre FM, Kerschensteiner M, Raineteau O, Mettenleiter TC, Weinmann O, Schwab ME. The injured spinal cord spontaneously forms a new intraspinal circuit in adult rats. Nat Neurosci 2004; 7: 269–77.

Barkhof F, Hulst HE, Drulovic J, Uitdehaag BM, Matsuda K, Landin R. Ibudilast in relapsing-remitting multiple sclerosis: a neuroprotectant? Neurology 2010; 74: 1033–40.

Beaud ML, Schmidlin E, Wannier T, Freund P, Bloch J, Mir A, et al. Anti-Nogo-A antibody treatment does not prevent cell body shrinkage in the motor cortex in adult monkeys subjected to unilateral cervical cord lesion. BMC Neurosci 2008; 9: 5.

Calancie B, Lutton S, Broton JG. Central nervous system plasticity after spinal cord injury in man: interlimb reflexes and the influence of cutaneous stimulation. Electroencephalogr Clin Neurophysiol 1996; 101: 304–15.

Ciccarelli O, Toosy AT, Marsden JF, Wheeler-Kingshott CM, Sahyoun C, Matthews PM, et al. Identifying brain regions for integrative sensorimotor processing with ankle movements. Exp Brain Res 2005; 166: 31–42.

Curt A, Alkadhi H, Crelier GR, Boendermaker SH, Hepp-Reymond MC, Kollias SS. Changes of non-affected upper limb cortical representation in paraplegic patients as assessed by fMRI. Brain 2002; 125: 2567–78.

Deichmann R, Schwarzbauer C, Turner R. Optimisation of the 3D MDEFT sequence for anatomical brain imaging: technical implications at 1.5 and 3 T. Neuroimage 2004; 21: 757–67.

Dietz V, Curt A. Neurological aspects of spinal-cord repair: promises and challenges. Lancet Neurol 2006; 5: 688–94.

Duggal N, Rabin D, Bartha R, Barry RL, Gati JS, Kowalczyk I, et al. Brain reorganization in patients with spinal cord compression evaluated using fMRI. Neurology 2010; 74: 1048–54.

Dusart I, Schwab ME. Secondary cell death and the inflammatory reaction after dorsal hemisection of the rat spinal cord. Eur J Neurosci 1994; 6: 712–24.

Elbert T, Pantev C, Wienbruch C, Rockstroh B, Taub E. Increased cortical representation of the fingers of the left hand in string players. Science 1995; 270: 305–7.

Ellaway PH, Kuppuswamy A, Balasubramaniam AV, Maksimovic R, Gall A, Craggs MD, et al. Development of quantitative and sensitive assessments of physiological and functional outcome during recovery from spinal cord injury: a clinical initiative. Brain Res Bull 2010; 84: 343–57.

Ferretti A, Babiloni C, Gratta CD, Caulo M, Tartaro A, Bonomo L, et al. Functional topography of the secondary somatosensory cortex for nonpainful and painful stimuli: an fMRI study. Neuroimage 2003; 20: 1625–38.

Fields RD. White matter in learning, cognition and psychiatric disorders. Trends Neurosci 2008; 31: 361–70.

Freund P, Schmidlin E, Wannier T, Bloch J, Mir A, Schwab ME, et al. Nogo-A-specific antibody treatment enhances sprouting and functional recovery after cervical lesion in adult primates. Nat Med 2006; 12: 790–2.

Freund P, Ward NS, Ciccarelli O, Friston K, Craggs M, Weiskopf N, et al. Chronic spinal cord injury results in cervical atrophy and topographical reorganization of affected upper limb muscles during handgrib. San Diego: Society for Neuroscience; 2009. Poster#: 542.22/T1.

Freund PA, Dalton C, Wheeler-Kingshott CA, Glensman J, Bradbury D, Thompson AJ, et al. Method for simultaneous voxel-based morphometry of the brain and cervical spinal cord area measurements using 3D-MDEFT. J Magn Reson Imaging 2010; 32: 1242–7.

Friston KJ, Holmes AP, Poline JB, Grasby PJ, Williams SC, Frackowiak RS, et al. Analysis of fMRI time-series revisited. Neuroimage 1995a; 2: 45–53.

Friston KJ, Holmes AP, Worsley KJ, Poline JB, Frith CD, Frackowiak RSJ. Statistical parametric maps in functional im aging: a general linear approach. Hum Brain Mapp 1995b; 2: 189–210.

Ghosh A, Haiss F, Sydekum E, Schneider R, Gullo M, Wyss MT, et al. Rewiring of hindlimb corticospinal neurons after spinal cord injury. Nat Neurosci 2010; 13: 97–104.

Hains BC, Black JA, Waxman SG. Primary cortical motor neurons undergo apoptosis after axotomizing spinal cord injury. J Comp Neurol 2003; 462: 328–41.

Hoogervorst EL, Kalkers NF, Uitdehaag BM, Polman CH. A study validating changes in the multiple sclerosis functional composite. Arch Neurol 2002; 59: 113–6.

Hutton C, De VE, Ashburner J, Deichmann R, Turner R. Voxel-based cortical thickness measurements in MRI. Neuroimage 2008; 40: 1701–10.

Hutton C, Draganski B, Ashburner J, Weiskopf N. A comparison between voxel-based cortical thickness and voxel-based morphometry in normal aging. Neuroimage 2009; 48: 371–80.

Jain N, Florence SL, Qi HX, Kaas JH. Growth of new brainstem connections in adult monkeys with massive sensory loss. Proc Natl Acad Sci USA 2000; 97: 5546–50.

Jones EG. Cortical and subcortical contributions to activity-dependent plasticity in primate somatosensory cortex. Annu Rev Neurosci 2000; 23: 1–37.

Josephs O, Deichmann R, Turner R. Trajectory measurement and generalised reconstruction in rectilinear EPI. In: Proceedings of International Society for Magnetic Resonance in Medicine 8, Denver, CO. 2000. p. 1517.

Jurkiewicz MT, Crawley AP, Verrier MC, Fehlings MG, Mikulis DJ. Somatosensory cortical atrophy after spinal cord injury: a voxel-based morphometry study. Neurology 2006; 66: 762–4.

Jurkiewicz MT, Mikulis DJ, Fehlings MG, Verrier MC. Sensorimotor cortical activation in patients with cervical spinal cord injury with persisting paralysis. Neurorehabil Neural Repair 2010; 24: 136–40.

Jurkiewicz MT, Mikulis DJ, McIlroy WE, Fehlings MG, Verrier MC. Sensorimotor cortical plasticity during recovery following spinal cord injury: a longitudinal fMRI study. Neurorehabil Neural Repair 2007; 21: 527–38.

Kim BG, Dai HN, McAtee M, Vicini S, Bregman BS. Remodeling of synaptic structures in the motor cortex following spinal cord injury. Exp Neurol 2006; 198: 401–15.

Kokotilo KJ, Eng JJ, Curt A. Reorganization and preservation of motor control of the brain in spinal cord injury: a systematic review. J Neurotrauma 2009; 26: 2113–26.

Losseff NA, Webb SL, O'Riordan JI, Page R, Wang L, Barker GJ, et al. Spinal cord atrophy and disability in multiple sclerosis. A new reproducible and sensitive MRI method with potential to monitor disease progression. Brain 1996; 119 (Pt 3): 701–8.

Lundell H, Barthelemy D, Skimminge A, Dyrby TB, Biering-Sorensen F, Nielsen JB. Independent spinal cord atrophy measures correlate to motor and sensory deficits in individuals with spinal cord injury. Spinal Cord 2011a; 49: 70–5.

Lundell H, Christensen MS, Barthelemy D, Willerslev-Olsen M, Biering-Sorensen F, Nielsen JB. Cerebral activation is correlated to regional atrophy of the spinal cord and functional motor disability in spinal cord injured individuals. Neuroimage 2011b; 54: 1254–61.

Lyle RC. A performance test for assessment of upper limb function in physical rehabilitation treatment and research. Int J Rehabil Res 1981; 4: 483–92.

Moore CI, Stern CE, Dunbar C, Kostyk SK, Gehi A, Corkin S. Referred phantom sensations and cortical reorganization after spinal cord injury in humans. Proc Natl Acad Sci USA 2000; 97: 14703–8.

Mori S, Oishi K, Jiang H, Jiang L, Li X, Akhter K, et al. Stereotaxic white matter atlas based on diffusion tensor imaging in an ICBM template. Neuroimage 2008; 40: 570–82.

Nudo RJ, Wise BM, SiFuentes F, Milliken GW. Neural substrates for the effects of rehabilitative training on motor recovery after ischemic infarct. Science 1996; 272: 1791–4.

Schwab ME. Repairing the injured spinal cord. Science 2002; 295: 1029–31.

Shoham S, Halgren E, Maynard EM, Normann RA. Motor-cortical activity in tetraplegics. Nature 2001; 413: 793.

Talelli P, Ewas A, Waddingham W, Rothwell JC, Ward NS. Neural correlates of age-related changes in cortical neurophysiology. Neuroimage 2008; 40: 1772–81.

Tseng GF, Prince DA. Structural and functional alterations in rat corticospinal neurons after axotomy. J Neurophysiol 1996; 75: 248–67.

Turner JA, Lee JS, Schandler SL, Cohen MJ. An fMRI investigation of hand representation in paraplegic humans. Neurorehabil Neural Repair 2003; 17: 37–47.

Ward NS, Frackowiak RS. Age-related changes in the neural correlates of motor performance. Brain 2003; 126: 873–88.

Weiskopf N, Sitaram R, Josephs O, Veit R, Scharnowski F, Goebel R, et al. Real-time functional magnetic resonance imaging: methods and applications. Magn Reson Imaging 2007; 25: 989–1003.

Wrigley PJ, Gustin SM, Macey PM, Nash PG, Gandevia SC, Macefield VG, et al. Anatomical changes in human motor cortex and motor pathways following complete thoracic spinal cord injury. Cereb Cortex 2009a; 19: 224–32.

Wrigley PJ, Press SR, Gustin SM, Macefield VG, Gandevia SC, Cousins MJ, et al. Neuropathic pain and primary somatosensory cortex reorganization following spinal cord injury. Pain 2009b; 141: 52–9.